Concepts and preliminaries

The Earth is the cradle of humanity, but mankind cannot stay in the cradle forever.

Konstantin Tsiolkovsky, *pioneer of the astronautic theory*

Chapitre 4

Polytropic sheath model in the presence of electron emission

We add to the non-isothermal sheath model developed in Chapter 3 the secondary electron emission. Using the Particle in Cell (PIC) simulations, we observe that the polytropic index is almost constant when varying the cross-over energy ϵ^*. We note that this model allows multiple solutions for a given electron temperature, which could explain the oscillations observed in regime **II**. The predictions of the polytropic sheath model are successfully compared to the PIC simulations results presented in Chapter 2.

Contents

A lire

Sydorenko et al. [60] : non maxwellian EVDF
Raitses et al. [61] : electron-wall interaction
Jolivet and Roussel [62] : SEE effect on EVDF

4.1 Polytropic index in the HET PIC simulations

We have developed in Chapter 3 a sheath model that uses a polytropic state law for the electrons instead of the usual isothermal approximation. This model successfully reproduced the sheath characteristics when no secondary electron emission where present (fully absorbing walls). We now include the effects of the electron emission from the wall.

In this chapter, the PIC simulations are the same as in Section 2.4. Hence, the dielectric electrostatic boundary condition is not modeled, but instead the walls are grounded. In addition, we recall that the axial convection is model using Lafleur's model of convection, as discussed in Section 1.6.

4.1.1 Polytropic index determination from the PIC simulations

As previously done, we uses the mean values of the electron density n_e and the electron pressure $p_e = n_e T_e$ to find the value of the polytropic index. Figure 4.1 shows the radial profiles of the electron density and temperature for different values of the cross-over energy ϵ^*. The three values of ϵ^* are representative of the behaviour observed. Indeed, $\epsilon^* = 200\,\mathrm{V}$ and $\epsilon^* = 50\,\mathrm{V}$ correspond to the upper and lower limits of regime **III**, corresponding to low emission rate $\bar{\sigma}$, while regime **I** corresponds to the case $\epsilon^* = 10\,\mathrm{V}$. Regime **II** is not presented has the oscillating nature of the sheath is not taken into account by the stationary sheath modeled developed here.

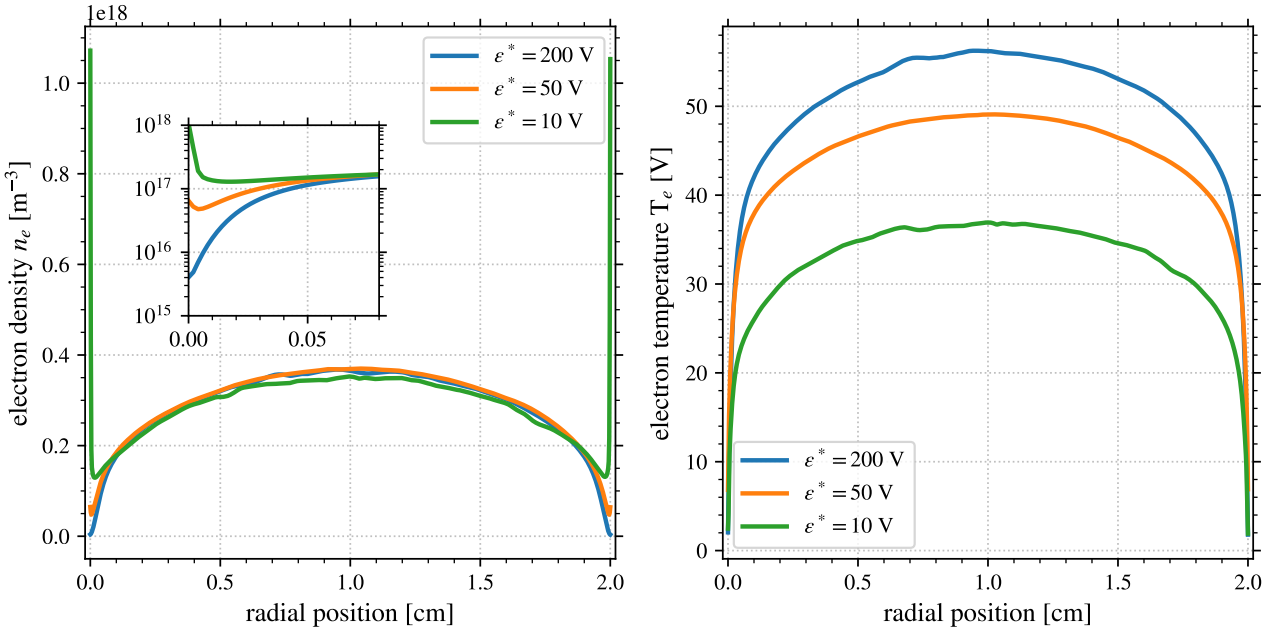

FIGURE 4.1 – Radial profiles of (left) the electron density and (right) the electron temperature, for different values of ϵ^*. The variables are averaged over the azimuthal direction and in time between $t = 5\,\mu\mathrm{s}$ and $t = 10\,\mu\mathrm{s}$.

We can see that the electron temperature presents a monotonic profile for all the values of ϵ^*. However, the electron density is not monotonic, but instead presents an increase close to the wall. This is clearly visible in Fig. 4.2 that presents the electron pressure p_e as a function of the electron density n_e, in log scale. We see that close to the wall, where the electron pressure is the lowest, the curves present an inversion, in contrast with the case without electron emission seen in Fig. 3.9. Otherwise in the rest of the domain, the curves are almost linear, corresponding to a polytropic law.

We compute the value of the polytropic index γ from the PIC simulations with a least mean square linear regression. The results of the regressions are displayed in Fig. 4.3. We can see that the value of γ do not evolve significantly in regime **III**, as it evolves from $\gamma = 1.35$ for $\epsilon^* = 200\,\mathrm{V}$ to $\gamma = 1.37$ for $\epsilon^* = 200\,\mathrm{V}$. For $\epsilon^* = 10\,\mathrm{V}$, the value of the polytropic index, in the linear stage, is $\gamma = 1.59$, which is not so different from regime **III**.

Consequently, we can suppose that the polytropic index in the PIC simulation with secondary electron emission is constant, and equals $\gamma = 1.36$. This value will be used in the next sections to compare the PIC results with a fluid model of the sheath.

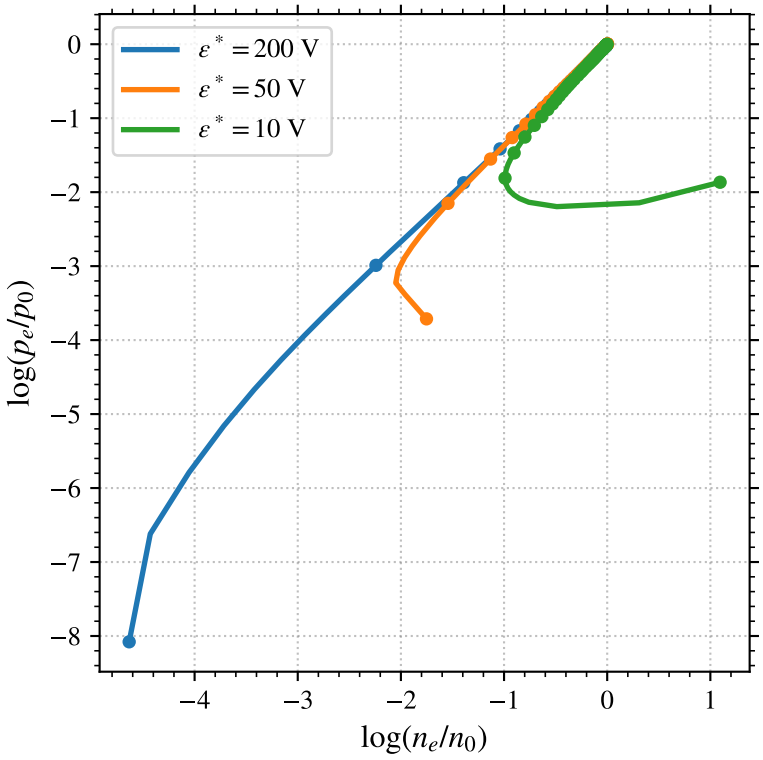

FIGURE 4.2 – Electron pressure as a function of the electron density normalized by the center variable, in log scale. The data corresponds to the same as Fig. 4.1. Markers are used every 10 cells (corresponding to around one Debye length λ_{De})

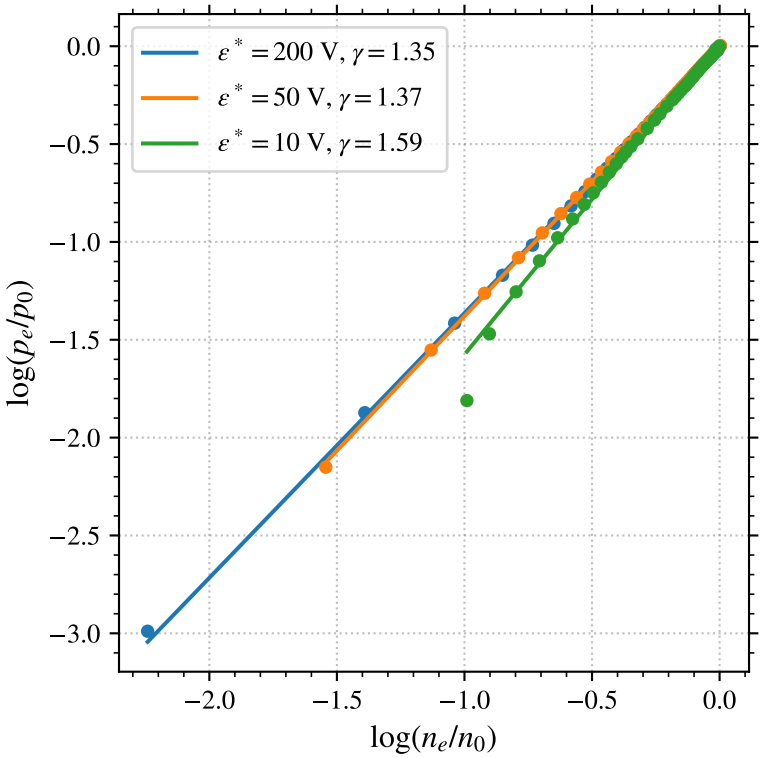

FIGURE 4.3 – Polytropic fit for different values of ϵ^*, in the same conditions that Fig. 4.2, but the last 10 cells near the wall are removed, the value of γ fitted on the PIC simulation data is given in the legend.

4.1.2 Evolution of the electron distribution function

Figure 4.4 presents the electron distribution functions measured at the center of the simulation.

Is it the center or the sheath-edge ?

We can see that the Electron Velocity Distribution Function (EVDF) presents similar profiles for the three cases, except for the mean energy that decreases with increasing value of ϵ^*.

We can note that no beam is present here, even in the case of very large electron emission at $\epsilon^* = 10\,\mathrm{V}$, in contrast with observations of 1 dimension (1D) PIC simulations [24, 60] but in agreement with the 2 dimensions (2D) results of Héron and Adam [15].

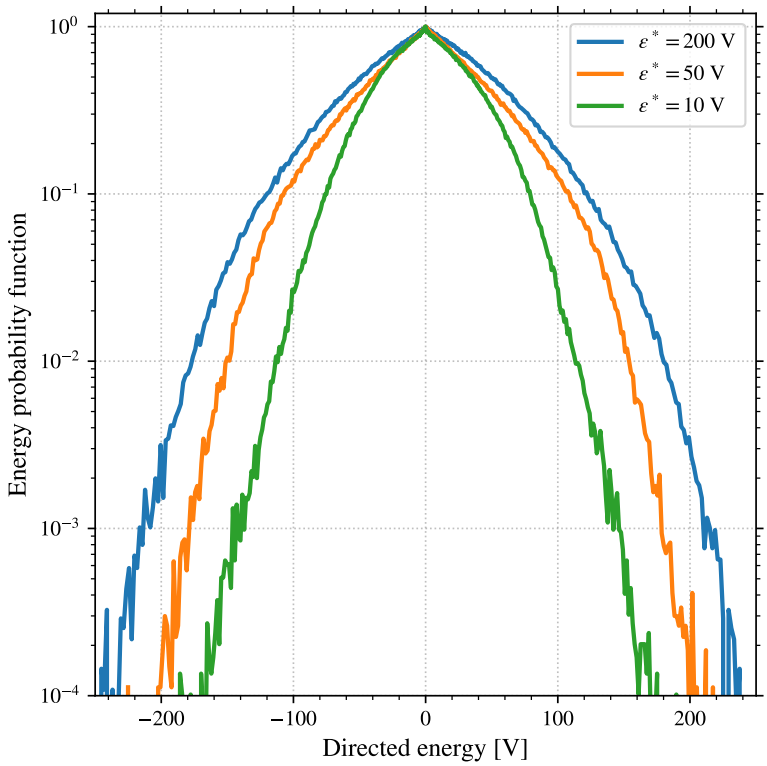

FIGURE 4.4 – Electron velocity distribution function at the center of the simulation, for different values of ϵ^*.

Using the solution of the stationary Vlasov equation Eq. (3.16), we compute the evolution of the density and temperature of the electron population going toward the wall. The results is compared to the mean density and temperature measured in the PIC simulations in Fig. 4.5.

We can see that the pressure of the forward electron population decreases slower than the total electrons. The may be due to the partial absorption and emission of secondary electrons at the wall, injected at $\mathrm{T_{SEE}} = 2\,\mathrm{V}$. Hence, we can expect that the emission rate σ, which directly depends on the forward electron population, to be better decreased with the polytropic index computed in Fig. 4.5 than in Section 4.1.1.

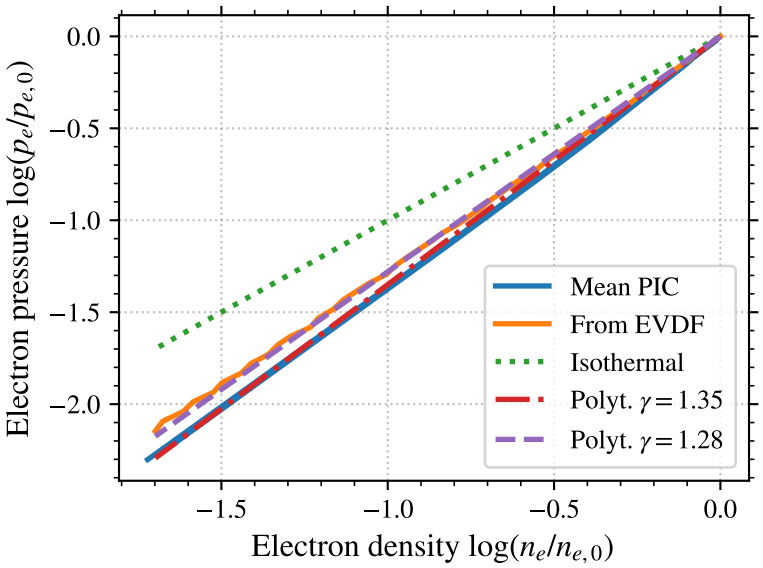

FIGURE 4.5 – Pressure and density in log scale of (orange) the forward electron using the stationary Vlasov equation, compared with (blue) the values measured in the PIC simulations, for $\epsilon^* = 200\,\mathrm{V}$. Different polytropic models are given as well (the isothermal corresponds to $\gamma = 1$).

4.2 Sheath model with polytropic electron and electron emission

We have seen in Section 4.1 that even in the presence of electron emission from the wall, the electrons can be decreased using a polytropic state law. The value of the polytropic index obtained from the mean electron density and temperature is for $\epsilon^* \geq 40\,\mathrm{V}$ is $\gamma = 1.35$.

Hence, we modify the polytropic sheath model of Section 3.5 to take into account the electron emission fromthe wall. This modify the current equality at the wall to

$$J_i = (1 - \bar{\sigma}) J_e. \tag{4.1}$$

Using Eqs. (3.30), (3.32) and (3.33), we obtain the equality

$$(1 - \bar{\sigma}) \left[1 + \frac{\gamma - 1}{\gamma} \frac{\Delta\phi_0}{\mathrm{T_{e0}}}\right]^{\frac{1}{\gamma - 1}} \sqrt{1 - \frac{\gamma - 1}{\gamma} \frac{\Delta\phi_0}{\mathrm{T_{e0}}}} = \sqrt{\frac{4\gamma\pi m_e}{m_i}} \tag{4.2}$$

As in the case without electron emission, Eq. (4.2) cannot be solved analytically, but it can be solved numerically.

The solution for $\bar{\sigma} = 0.8$ is compared to the case without electron emission for a Xenon (Xe) plasma in Fig. 4.6. As expected, the potential difference decrease with increasing $\bar{\sigma}$, but the difference decreases with increases γ.

The electron emission rate is actually a function of the electron energy at the wall. Hence, using the same hypothesis that used in Eq. (3.32), we can compute the emission rate with Eq. (2.11)

$$\bar{\sigma} = \bar{\sigma}_{\mathrm{Maxw}}(\mathrm{T_{e,wall}}) = \sigma_0 + (1 - \sigma_0) \frac{2\mathrm{T_{e,wall}}}{\epsilon^*}. \tag{4.3}$$

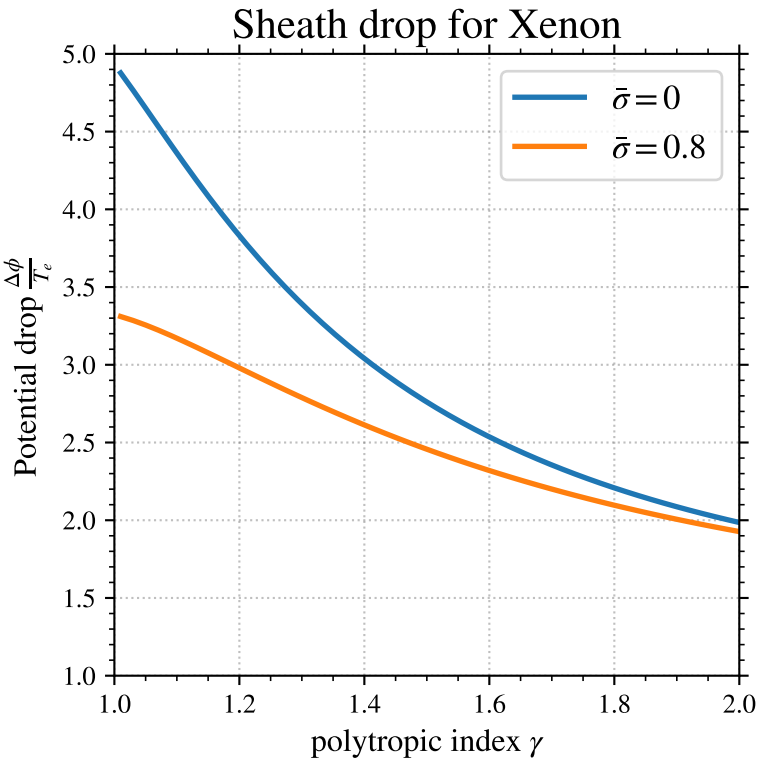

FIGURE 4.6 – Potential drop $\Delta\phi$ normilized by the bulk electron temperature T_{e0} as a function of the polytropic index γ for a xenon plasma ($m_i = 131\,\mathrm{u}$). The emission rate $\bar{\sigma}$ is fixed for clarity.

Combined with Eq. (3.33), we obtain

$$\bar{\sigma} = \sigma_0 + (1-\sigma_0)\frac{2\left(\mathrm{T_{e,0}} - \frac{\gamma-1}{\gamma}\Delta\phi\right)}{\epsilon^*}. \tag{4.4}$$

Here, for sake of clarity we do not write the saturation of $\bar{\sigma}$ to $\bar{\sigma}_{\mathrm{cr}}$ due to the Space Charge Limit (SCL) regime. However, we include it the the next calculations.

Noting $\chi = \frac{\gamma-1}{\gamma}\frac{\Delta\phi_0}{\mathrm{T_{e0}}}$, we finely obtain the equation to be solved

$$[1+\chi]^{\frac{1}{\gamma-1}}\sqrt{1-\chi} - \frac{\epsilon^*\sqrt{4\gamma m_e/m_i}}{2\mathrm{T_{e,0}}(1-\sigma_0)[1-(1-\chi)]} = 0. \tag{4.5}$$

Equation (4.5) depends explicitly on $\mathrm{T_{e,0}}$, hence χ is no longer independent of $\mathrm{T_{e,0}}$. Moreover, the Right Hand Side (RHS) of Eq. (4.5) is more complex that before, leading to multiple solutions. Figure 4.7 shows the RHS of Eq. (4.5) for several values of (**a**) $\mathrm{T_{e,0}}$ and (**b**) ϵ^*, while keeping the polytropic index to $\gamma = 1.35$.

The SCL regime has been taken into account by saturating $\bar{\sigma}$ to $\bar{\sigma}_{\mathrm{cr}} = 0.982$. It corresponds to the branch which crosses the abscissa axis close to $\frac{\Delta\phi}{\mathrm{T_{e,0}}} = 1$.

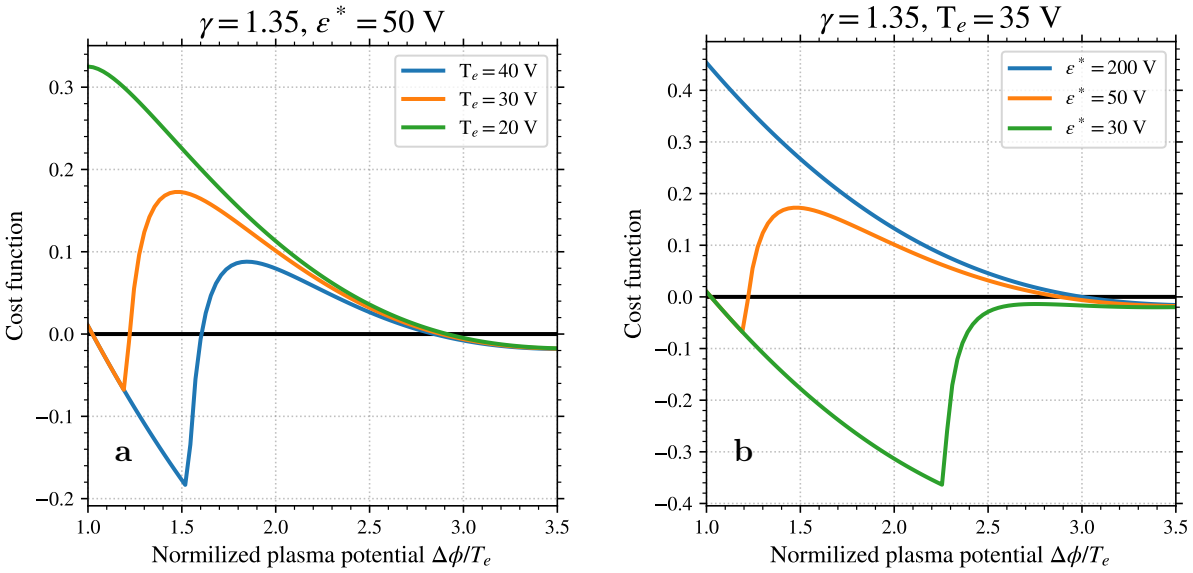

FIGURE 4.7 – Value of the RHS of Eq. (4.5), labelled cost function, for several values of (**a**) $\mathrm{T_{e,0}}$ and (**b**) ϵ^*.

We can see that Eq. (4.5) can present one or three solutions, depending of the relative values of *crover* and $\mathrm{T_{e,0}}$. Hence, a particular care must be taken now when finding numerically the sheath potential drop.

Figure 4.8 shows the evolution of the sheath potential drop with the electron temperature for different values of ϵ^*. It is similar to Fig. 2.14 but with the use of a polytropic state law for the electrons. Two main aspects differ compared to the isothermal model: the multiple solutions and the maximal electron temperature of the first solution.

We observe in Fig. 4.8 that the electron temperature in the center $\mathrm{T_{e,0}}$ can be much higher before the inversion of the plasma sheath potential, compared to Fig. 2.14. Indeed, the

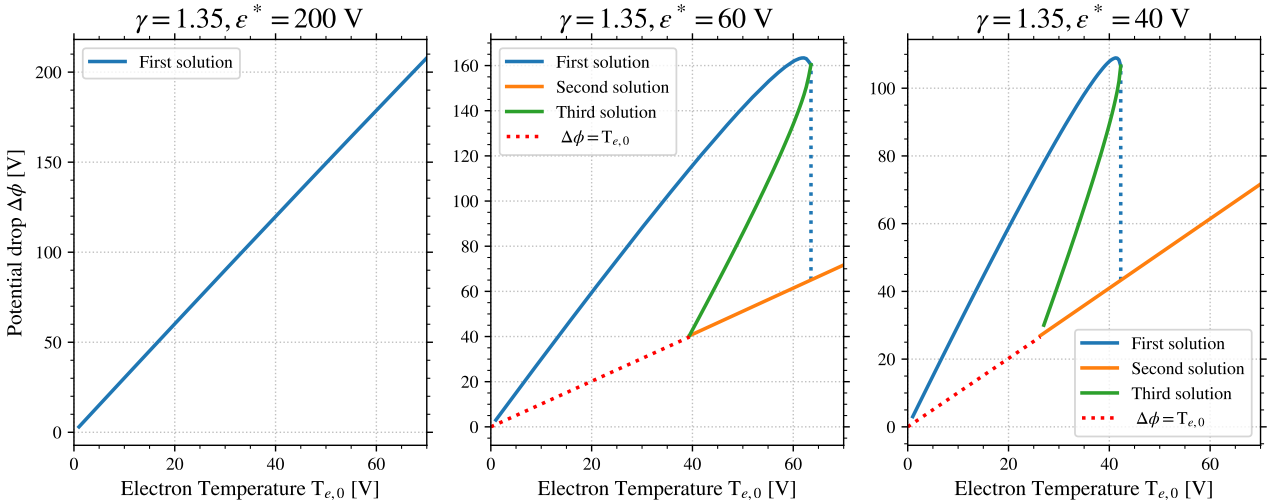

FIGURE 4.8 – Plasma potential drop to the wall as a function of the electron temperature for different values of the cross-over energy ϵ^* using Eq. (4.5). It is the same results as Fig. 2.14 but with polytropic electron of index $\gamma = 1.35$.

polytropic state law reduces the electron temperature at the wall, hence decreases the electron emission rate for a given $T_{e,0}$. Consequently, the electron bulk temperature can access higher temperature, compared to the one observed in Fig. 2.14. Moreover, we see that the critical temperature for $\epsilon^* = 40$ V is close to $T_e = 40$ V, which is consistent with the transition between the regimes **III** and **II** observed in the PIC simulations.

In addition, for some values of electron temperature, there are three solutions. This could explain the oscillations observed in regime **II**. Indeed, when the electron temperature increases, the sheath follows the first solutions. When the critical electron temperature, the sheath jump to the third solution. It corresponds to the SCL regime with an inverted sheath. There, the electron temperature in the bulk decreases because of the increased electron power losses at the wall. The electron temperature decreases until the second critical temperature, which corresponds to the moment when the third solution disappear, so that the sheath jumps back to the first solution. We do not expect the third solution in-between to be observed in the simulations.

Obviously, the current model suppose that the polytropic index is constant. However, we saw in the PIC simulations that it increases from $\gamma = 1.34$ to 1.59. Hence, the exact values of the critical temperature may not exactly correspond to the one observed in the simulations. On the other hand, we can expect the overall behaviour not to be significantly affected.

To summarize, the polytropic law is combined with electron emission to model the sheath. The model is richer than the usual isothermal model, as it allows multiple values of potential drop to the wall for the same electron bulk temperature.

This model only uses the electron bulk temperature and self-consistently compute both the potential drop and the electron emission rate. It is compared in the next section to the PIC simulation results.

4.3 Comparison of the sheath model with PIC simulations

We compare in this section the characteristics of the plasma wall interaction observed in the PIC simulations with the fluid model developed in Section 4.2. The variables of interest are the averaged electron emission rate $\bar{\sigma}$ and the plasma potential drop to the wall. The only input of the model is the electron mean temperature in the bulk $T_{e,0}$ as well as the polytropic index γ. As seen in Section 4.1, the polytropic index of the electron population is measured in the PIC simulation to $\gamma = 1.35$. However, the electrons going toward the wall present a different index, measured from the bulk EVDF to $\gamma = 1.28$. These two values will be compared.

Using the mean electron temperature measured in the simulation, we first compute the plasma potential drop $\Delta\phi$ by solving Eq. (4.5) with $\gamma = 1.35$. As showed in Fig. 4.8, up to three solutions are possible. The emission rate $\bar{\sigma}$ is then computed using Eq. (4.4), using the two values for γ. As discussed previously, the rate is limited to $\bar{\sigma}_{cr} = 0.982$ to take into account the SCL regime.

The results are shown in Figure 4.9. The plasma potential drop computed is increased by $T_{e,0}/2$ corresponding to the pre-sheath drop to better match the plasma potential measured in the simulations.

The Bhom criterion is slightly modified with the polytropic model, so it should not exactly be $T_{e,0}/2$. however, it matches to well here that I do not really want to change !

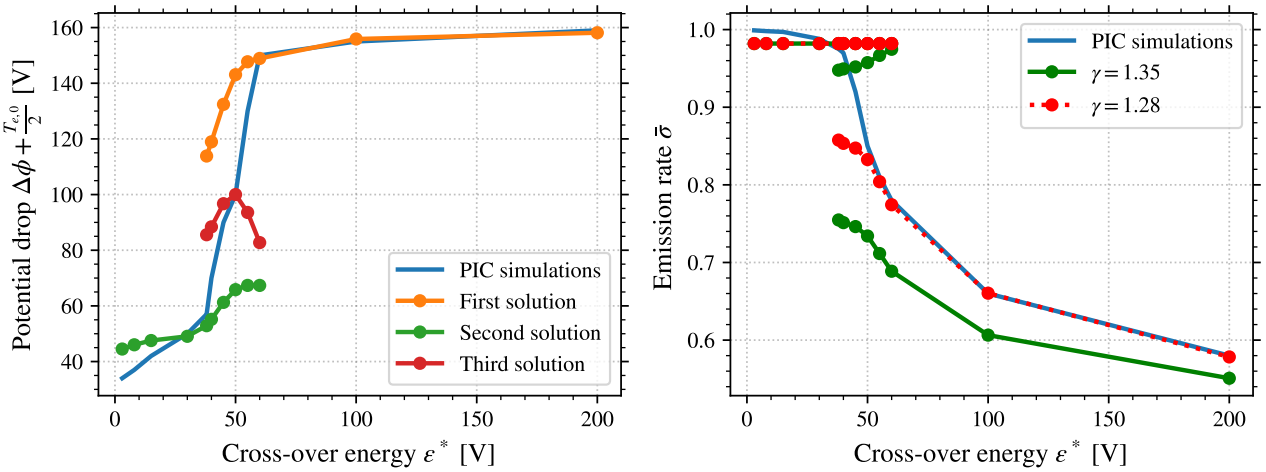

FIGURE 4.9 – Comparison of the PIC simulations and the sheath model for the plasma potential drop from the center to the wall and the electron emission yield.

Concerning $\Delta\phi$, we can see that the sheath model combining the polytropic state law and the electron emission is in good agreement with the PIC simulations. We can see that the region where the three solutions coexist corresponds well with the regime **II**.

For the emission rate $\bar{\sigma}$, we observe that the value $\gamma = 1.35$ under estimates $\bar{\sigma}$ compared to the values of the PIC simulations. On the other hand, $\gamma = 1.28$ is in very good agreement.

Interestingly, at the saturation the mean electron emission rate in the PIC simulation is greater than the critical value $\bar{\sigma}_{cr}$.

As $\bar{\sigma}$ is better with $\gamma = 1.28$, we should use both values in Eq. (4.5). However, this increases the complexity the equations and the model, and add 1 more free parameters (they would be 2 values for γ now). I can say that only in the discussion maybe ?

Annexe A

Bibliographie

[1] S. Barral, K. Makowski, Z. Peradzyński, N. Gascon, and M. Dudeck. Wall material effects in stationary plasma thrusters. II. Near-wall and in-wall conductivity. *Physics of Plasmas*, 10(10) :4137–4152, 2003.

[2] D Gawron, S Mazouffre, N Sadeghi, and A Héron. Influence of magnetic field and discharge voltage on the acceleration layer features in a Hall effect thruster. *Plasma Sources Science and Technology*, 17(2) :025001, 2008.

[3] T. Lafleur, S. D. Baalrud, and P. Chabert. Theory for the anomalous electron transport in Hall effect thrusters. I. Insights from particle-in-cell simulations. *Physics of Plasmas*, 23(5) :053502, 2016.

[4] Francis F. Chen and Francis F. Chen. *Plasma Physics*. Number Francis F. Chen ; Vol. 1 in Introduction to Plasma Physics and Controlled Fusion. Springer US, New York, 2. ed., 5. printing edition, 2006. OCLC : 836567560.

[5] Nathan B. Meezan, William A. Hargus, and Mark A. Cappelli. Anomalous electron mobility in a coaxial Hall discharge plasma. *Physical Review E*, 63(2), 2001.

[6] Hiroko Ueda, Yoshiharu Omura, Hiroshi Matsumoto, and Takashi Okuzawa. A study of the numerical heating in electrostatic particle simulations. *Computer physics communications*, 79(2) :249–259, 1994.

[7] Salomon Janhunen, Andrei Smolyakov, Dmytro Sydorenko, Marilyn Jimenez, Igor Kaganovich, and Yevgeny Raitses. Evolution of the electron cyclotron drift instability in two-dimensions. *Physics of Plasmas*, 25(8) :082308, 2018.

[8] V. Vahedi, M. A. Lieberman, G. DiPeso, T. D. Rognlien, and D. Hewett. Analytic model of power deposition in inductively coupled plasma sources. *Journal of Applied Physics*, 78 (3) :1446–1458, 1995.

[9] LXCat project. www.lxcat.net, 2019.

[10] A.V. Phelps. Phelps database. www.lxcat.net, retrieved on November 16 2016.

[11] Cross sections extracted program {MAGBOLTZ}. www.lxcat.net, version 7.1 june 2016.

[12] C. K. Birdsall. Particle-in-cell charged-particle simulations, plus Monte Carlo collisions with neutral atoms, PIC-MCC. *IEEE Transactions on Plasma Science*, 19(2) :65–85, 1991.

[13] J Boris. Relativistic plasma simulation-optimization of a hybrid code. In *Fourth Conference on Numerical Simulations of Plasmas*, 1970.

[14] Robert D. Falgout and Ulrike Meier Yang. Hypre : A Library of High Performance Preconditioners. In Gerhard Goos, Juris Hartmanis, Jan van Leeuwen, Peter M. A. Sloot, Alfons G. Hoekstra, C. J. Kenneth Tan, and Jack J. Dongarra, editors, *Computational Science — ICCS 2002*, volume 2331, pages 632–641. Springer Berlin Heidelberg, Berlin, Heidelberg, 2002.

[15] A. Héron and J. C. Adam. Anomalous conductivity in Hall thrusters : Effects of the non-linear coupling of the electron-cyclotron drift instability with secondary electron emission of the walls. *Physics of Plasmas*, 20(8) :082313, 2013.

[16] A Domínguez-Vázquez, F Taccogna, and E Ahedo. Particle modeling of radial electron dynamics in a controlled discharge of a Hall thruster. *Plasma Sources Science and Technology*, 27(6) :064006, 2018.

[17] Vivien Croes, Trevor Lafleur, Zdeněk Bonaventura, Anne Bourdon, and Pascal Chabert. 2D particle-in-cell simulations of the electron drift instability and associated anomalous electron transport in Hall-effect thrusters. *Plasma Sources Science and Technology*, 26 (3) :034001, 2017.

[18] Vivien Croes. *Modélisation bidimensionnelle de la décharge plasma dans un propulseur de Hall*. PhD thesis, Université Paris-Saclay, 2017.

[19] Oliver C. Ibe. 9 - Brownian Motion. In Oliver C. Ibe, editor, *Markov Processes for Stochastic Modeling (Second Edition)*, pages 263–293. Elsevier, Oxford, 2013.

[20] Marc Villemant. *Modélisation et caractérisation expérimentale de l'influence de l'émission électronique sur le fonctionnement des propulseurs à courant de Hall*. PhD thesis, Institut Supérieur de l'Aéronautique et de l'Espace (ISAE), 2018.

[21] M. Furman and M. Pivi. Probabilistic model for the simulation of secondary electron emission. *Physical Review Special Topics - Accelerators and Beams*, 5(12), 2002.

[22] J. Pierron, C. Inguimbert, M. Belhaj, T. Gineste, J Puech, and M. Raine. Electron emission yield for low energy electrons : Monte Carlo simulation and experimental comparison for Al, Ag, and Si. *Journal of Applied Physics*, 121(21) :215107, 2017.

[23] J.R.M. Vaughan. A new formula for secondary emission yield. *IEEE Transactions on Electron Devices*, 36(9) :1963–1967, Sept./1989.

[24] D. Sydorenko, A. Smolyakov, I. Kaganovich, and Y. Raitses. Modification of electron velocity distribution in bounded plasmas by secondary electron emission. *IEEE Transactions on Plasma Science*, 34(3) :815–824, 2006.

[25] J C Adam, J P Boeuf, N Dubuit, M Dudeck, L Garrigues, D Gresillon, A Heron, G J M Hagelaar, V Kulaev, N Lemoine, S Mazouffre, J Perez Luna, V Pisarev, and S Tsikata. Physics, simulation and diagnostics of Hall effect thrusters. *Plasma Physics and Controlled Fusion*, 50(12) :124041, 2008.

[26] G D Hobbs and J A Wesson. Heat flow through a Langmuir sheath in the presence of electron emission. *Plasma Physics*, 9(1) :85–87, 1967.

[27] E. Ahedo and F. I. Parra. Partial trapping of secondary-electron emission in a Hall thruster plasma. *Physics of Plasmas*, 12(7) :073503, 2005.

[28] E. Ahedo. Presheath/sheath model with secondary electron emission from two parallel walls. *Physics of Plasmas*, 9(10) :4340–4347, 2002.

[29] Dan M Goebel and Ira Katz. *Fundamentals of Electric Propulsion : Ion and Hall Thrusters*. JPL Space Science and Technology Series. Jet Propulsion Laboratory, California Institute of Technology, 2008.

[30] P Chabert. What is the size of a floating sheath ? *Plasma Sources Science and Technology*, 23(6) :065042, 2014.

[31] T. Lafleur, S. D. Baalrud, and P. Chabert. Theory for the anomalous electron transport in Hall effect thrusters. II. Kinetic model. *Physics of Plasmas*, 23(5) :053503, 2016.

[32] T Lafleur, S D Baalrud, and P Chabert. Characteristics and transport effects of the electron drift instability in Hall-effect thrusters. *Plasma Sources Science and Technology*, 26(2) :024008, 2017.

[33] A. I. Morozov. Wall conduction in a highly magnetized plasma. *Journal of Applied Mechanics and Technical Physics*, 9(3) :249–251, 1972.

[34] Y. Raitses, D. Staack, A. Smirnov, and N. J. Fisch. Space charge saturated sheath regime and electron temperature saturation in Hall thrusters. *Physics of Plasmas*, 12(7) :073507, 2005.

[35] Y Raitses, I D Kaganovich, A Khrabrov, D Sydorenko, N J Fisch, and A Smolyakov. Effect of Secondary Electron Emission on Electron Cross-Field Current in $E \times B$ Discharges. *IEEE Transactions on Plasma Science*, 39(4) :995–1006, 2011.

[36] Dmytro Sydorenko. *Particle-in-Cell Simulations of Electron Dynamics in Low Pressure Discharges with Magnetic Fields*. PhD thesis, University of Saskatchewan, 2006.

[37] Ira B. Bernstein and T. Holstein. Electron Energy Distributions in Stationary Discharges. *Physical Review*, 94(6) :1475–1482, 1954.

[38] V. A. Godyak and R. B. Piejak. Paradoxical spatial distribution of the electron temperature in a low pressure rf discharge. *Applied Physics Letters*, 63(23) :3137–3139, 1993.

[39] S Mouchtouris and G Kokkoris. A hybrid model for low pressure inductively coupled plasmas combining a fluid model for electrons with a plasma-potential-dependent energy distribution and a fluid-Monte Carlo model for ions. *Plasma Sources Science and Technology*, 25(2) :025007, 2016.

[40] V A Godyak, R B Piejak, and B M Alexandrovich. Electron energy distribution function measurements and plasma parameters in inductively coupled argon plasma. *Plasma Sources Science and Technology*, 11(4) :525–543, 2002.

[41] Albert Meige and Rod W. Boswell. Electron energy distribution functions in low-pressure inductively coupled bounded plasmas. *Physics of Plasmas*, 13(9) :092104, 2006.

[42] I. Kaganovich, M. Mišina, S. V. Berezhnoi, and R. Gijbels. Electron Boltzmann kinetic equation averaged over fast electron bouncing and pitch-angle scattering for fast modeling of electron cyclotron resonance discharge. *Physical Review E*, 61(2) :1875–1889, 2000.

[43] I. D. Kaganovich, Y. Raitses, D. Sydorenko, and A. Smolyakov. Kinetic effects in a Hall thruster discharge. *Physics of Plasmas*, 14(5) :057104, 2007.

[44] M. M. Turner, A. Derzsi, Z. Donkó, D. Eremin, S. J. Kelly, T. Lafleur, and T. Mussenbrock. Simulation benchmarks for low-pressure plasmas : Capacitive discharges. *Physics of Plasmas*, 20(1) :013507, 2013.

[45] Pascal Chabert and Nicholas Braithwaite. *Physics of Radio-Frequency Plasmas*. Cambridge University Press, 2011.

[46] T Lafleur, C Charles, and R W Boswell. Electron temperature characterization and power balance in a low magnetic field helicon mode. *Journal of Physics D : Applied Physics*, 44 (18) :185204, 2011.

[47] Yunchao Zhang, Christine Charles, and Rod Boswell. A Polytropic Model for Space and Laboratory Plasmas Described by Bi-Maxwellian Electron Distributions. *The Astrophysical Journal*, 829(1) :10, 2016.

[48] S. Kuhn, K.-U. Riemann, N. Jelić, D. D. Tskhakaya, D. Tskhakaya, and M. Stanojević. Link between fluid and kinetic parameters near the plasma boundary. *Physics of Plasmas*, 13(1) :013503, 2006.

[49] N. Jelić, K.-U. Riemann, T. Gyergyek, S. Kuhn, M. Stanojević, and J. Duhovnik. Fluid and kinetic parameters near the plasma-sheath boundary for finite Debye lengths. *Physics of Plasmas*, 14(10) :103506, 2007.

[50] M. J. Kushner. Monte-Carlo simulation of electron properties in rf parallel plate capacitively coupled discharges. *Journal of Applied Physics*, 54(9) :4958–4965, 1983.

[51] P. Y. Lai, T. Y. Lin, Y. R. Lin-Liu, and S. H. Chen. Numerical thermalization in particle-in-cell simulations with Monte-Carlo collisions. *Physics of Plasmas*, 21(12) :122111, 2014.

[52] John M. Dawson. Thermal Relaxation in a One-Species, One-Dimensional Plasma. *Physics of Fluids*, 7(3) :419, 1964.

[53] David Montgomery. Thermal Relaxation in One- and Two-Dimensional Plasma Models. *Physics of Fluids*, 13(5) :1405, 1970.

[54] M. M. Turner. Kinetic properties of particle-in-cell simulations compromised by Monte Carlo collisions. *Physics of Plasmas*, 13(3) :033506, 2006.

[55] K.-U. Riemann, J. Seebacher, D. D. Tskhakaya Sr, and S. Kuhn. The plasma–sheath matching problem. *Plasma Physics and Controlled Fusion*, 47(11) :1949, 2005.

[56] K U Riemann. The Bohm criterion and sheath formation. *Journal of Physics D : Applied Physics*, 24(4) :493–518, 1991.

[57] V. Demidov, C. DeJoseph, and A. Kudryavtsev. Anomalously High Near-Wall Sheath Potential Drop in a Plasma with Nonlocal Fast Electrons. *Physical Review Letters*, 95 (21), 2005.

[58] R. Lucken, V. Croes, T. Lafleur, J.-L. Raimbault, A. Bourdon, and P. Chabert. Edge-to-center plasma density ratios in two-dimensional plasma discharges. *Plasma Sources Science and Technology*, 27(3) :035004, 2018.

[59] M. M. Turner. Collisionless electron heating in an inductively coupled discharge. *Physical Review Letters*, 71(12) :1844–1847, 1993.

[60] D. Sydorenko, A. Smolyakov, I. Kaganovich, and Y. Raitses. Effects of non-Maxwellian electron velocity distribution function on two-stream instability in low-pressure discharges. *Physics of Plasmas*, 14(1) :013508, 2007.

[61] Y Raitses, D Staack, M Keidar, and N J Fisch. Electron-wall interaction in Hall thrusters. *Phys. Plasmas*, page 10, 2005.

[62] L. Jolivet and J.-F. Roussel. Effects of the secondary electron emission on the sheath phenomenon in Hall Thruster. In *International Conference on Spacecraft Propulsion*, Cannes, 2000.

[63] J. C. Adam, A. Héron, and G. Laval. Study of stationary plasma thrusters using two-dimensional fully kinetic simulations. *Physics of Plasmas*, 11(1) :295–305, 2004.

[64] A. Ducrocq, J. C. Adam, A. Héron, and G. Laval. High-frequency electron drift instability in the cross-field configuration of Hall thrusters. *Physics of Plasmas*, 13(10) :102111, 2006.

[65] Vivien Croes, Antoine Tavant, Romain Lucken, Roberto Martorelli, Trevor Lafleur, Anne Bourdon, and Pascal Chabert. The effect of alternative propellants on the electron drift instability in Hall-effect thrusters : Insight from 2D particle-in-cell simulations. *Physics of Plasmas*, 25(6) :063522, 2018.

[66] Francesco Taccogna, Pierpaolo Minelli, Zahra Asadi, and Guillaume Bogopolsky. Numerical studies of the ExB electron drift instability in Hall thrusters. *Plasma Sources Science and Technology*, 2019.

[67] Cyrille Honore, Sedina Tsikata, Dominique Gresillon, Anne Heron, Jordan Cavalier, and N. Lemoine. Hall Thruster small scale plasma fluctuations : Qualifying 2D PIC Simulations against Collective Scattering Experimental Data. In *Proceedings of the 32nd International Electric Propulsion Conference*, 2011.

[68] Jardan Cavalier. *Modèles cinétiques et caractérisation expérimentale des fluctuations électrostatiques dans un propulseur à effet Hall.* PhD thesis, Université de Lorraine, 2013.

[69] J. Cavalier, N. Lemoine, G. Bonhomme, S. Tsikata, C. Honoré, and D. Grésillon. Hall thruster plasma fluctuations identified as the E×B electron drift instability : Modeling and fitting on experimental data. *Physics of Plasmas*, 20(8) :082107, 2013.

[70] J. P. Boeuf and L. Garrigues. E × B electron drift instability in Hall thrusters : Particle-in-cell simulations vs. theory. *Physics of Plasmas*, 25(6) :061204, 2018.

[71] V N Tsytovich. *AN INTRODUCTION TO THE THEORY OF PLASMA TURBULENCE.* Pergamon Press, 1972.

[72] Gérard Belmont, Roland Grappin, Fabrice Mottez, Filippo Pantellini, and Guy Pelletier. *Collisionless Plasmas in Astrophysics : BELMONT :COLLISIONL.PLASM O-BK.* Wiley-VCH Verlag GmbH & Co. KGaA, Weinheim, Germany, 2013.

[73] Kentaro Hara. An overview of discharge plasma modeling for Hall effect thrusters. *Plasma Sources Science and Technology*, 28(4) :044001, 2019.

[74] T. Lafleur, R. Martorelli, P. Chabert, and A. Bourdon. Anomalous electron transport in Hall-effect thrusters : Comparison between quasi-linear kinetic theory and particle-in-cell simulations. *Physics of Plasmas*, 25(6) :061202, 2018.

[75] Burton D Fried and Samuel D Conte. The Plasma Dispersion Function. *Academic Press, New York and London*, page 424, 1961.

[76] Xie, Hua-Sheng. Generalized plasma dispersion function : One-solve-all treatment, visualizations, and application to Landau damping. *Physics of Plasmas*, 20(9) :092125, 2013.

[77] Salomon Janhunen, Andrei Smolyakov, Oleksandr Chapurin, Dmytro Sydorenko, Igor Kaganovich, and Yevgeni Raitses. Nonlinear structures and anomalous transport in partially magnetized $\mathbf{E\times B}$ plasmas. *Physics of Plasmas*, 25(1) :011608, 2018.

[78] Trevor Lafleur and Pascal Chabert. The role of instability-enhanced friction on 'anomalous' electron and ion transport in Hall-effect thrusters. *Plasma Sources Science and Technology*, 27(1) :015003, 2017.

[79] J A C Weideman. Computing the Hilbert Transform on the Real Line. *Mathematics of computation*, 64(210) :745 – 762, 1995.

[80] Steven Fortune. Polynomial root finding using iterated Eigenvalue computation. In *Proceedings of the 2001 International Symposium on Symbolic and Algebraic Computation - ISSAC '01*, pages 121–128, London, Ontario, Canada, 2001. ACM Press.

[81] K. I. M. McKinnon. Convergence of the Nelder–Mead Simplex Method to a Nonstationary Point. *SIAM Journal on Optimization*, 9(1) :148–158, 1998.

[82] M. J. D. Powell. An efficient method for finding the minimum of a function of several variables without calculating derivatives. *The Computer Journal*, 7(2) :155–162, 1964.

[83] E. E. Salpeter. Electron Density Fluctuations in a Plasma. *Physical Review*, 120(5) : 1528–1535, 1960.

[84] Kjell Rönnmark. WHAMP- WAVES IN HOMOGENEOUS, ANISOTROPIC MULTICOMPONENT PLASMAS. *KGI Report*, 179, 1982.